



Article

Characteristics of the Colorless Polyimide-Based Flexible X-ray Detector with Non-Fullerene Acceptor Polymer

Jehoon Lee ¹ , Jongkyu Won ¹, Duhee Lee ¹, Hailiang Liu ¹ and Jungwon Kang ^{1,2,*} 

¹ Department of Electronics and Electrical Engineering, Dankook University, Yongin-si 16890, Korea; usyj0512@gmail.com (J.L.); 1jongkyu@naver.com (J.W.); clemenslee94@gmail.com (D.L.); liuhailiang107@gmail.com (H.L.)

² Convergence Semiconductor Research Center, Dankook University, Yongin-si 16890, Korea

* Correspondence: jkang@dankook.ac.kr

Abstract: In this paper, we investigate the characteristics of the colorless polyimide (CPI) film-based flexible organic X-ray detector. The CPI film can be applied to various applications, because it shows excellent visible light transmittance by removing the yellow color of polyimide (PI) film, which has the advantage of physical and chemical stability. In addition, the deformation curvature of the CPI substrate according to temperature showed similar characteristics to that of the glass substrate. For the organic active layer of the proposed detector, PBDB-T was fixed as a donor, and PC₇₁BM and ITIC were used as acceptors. To evaluate the mechanical stability of the flexible detector, the degradation sensitivity was measured as bending curvature and bending cycle. The sensitivity of the detector with ITIC acceptor showed a 46.82% higher result than PC₇₁BM acceptor on bending curvature ($R = 10$); and at the same curvature, when the bending cycle was 500 times, a 135.85% higher result than PC₇₁BM acceptor.

Keywords: colorless polyimide; flexible detector; non-fullerene



Citation: Lee, J.; Won, J.; Lee, D.; Liu, H.; Kang, J. Characteristics of the Colorless Polyimide-Based Flexible X-ray Detector with Non-Fullerene Acceptor Polymer. *Nanomaterials* **2022**, *12*, 918. <https://doi.org/10.3390/nano12060918>

Academic Editors: Jun Chen and Placido Mineo

Received: 18 January 2022

Accepted: 8 March 2022

Published: 10 March 2022

Publisher's Note: MDPI stays neutral with regard to jurisdictional claims in published maps and institutional affiliations.



Copyright: © 2022 by the authors. Licensee MDPI, Basel, Switzerland. This article is an open access article distributed under the terms and conditions of the Creative Commons Attribution (CC BY) license (<https://creativecommons.org/licenses/by/4.0/>).

1. Introduction

Recently, flexible devices are attracting attention from industry and consumers due to their lightweight, bendable, and non-breakable properties. When flexible plastic substrates are applied, solution process-based roll-to-roll and inkjet methods are possible, and economical advantages of facile manufacture can be obtained. Due to these advantages, they are applied in various applications, such as solar cells [1], organic light-emitting diodes (OLED) [2], organic thin-film transistors (OFET) [3], and radiation detectors [4]. In particular, radiation detector applications are found in non-destructive testing, security, and medicine. A commonly used radiation detector is the rigid flat plate-type, and when measuring curved human bodies and objects, image distortion occurs. Therefore, by applying flexible properties to radiation detectors, image distortion can be overcome in non-destructive testing, and in medical applications, such as dental, mammography, and computerized tomography. In addition, because of its flexible characteristics, it is convenient to store and carry, and has the advantage of being able to measure the image of an object at once, because it can be enlarged in a relatively easy process. Flexible radiation detectors can be manufactured using plastic substrates, such as polyethylene terephthalate (PET) [5], polyethylene naphthalate (PEN) [6], and colorless polyimide (CPI) [7].

X-ray detection methods can be classified into two detection methods: indirect and direct. The direct method has the advantage of high spatial resolution, but it is difficult to use inorganic materials in the process, such as silicon, amorphous selenium, and cadmium telluride. On the other hand, the indirect method has the advantage of high detection efficiency and since the active layer can be composed of organic or organic/inorganic semiconductors, it allows simple device fabrication, measurement, and evaluation [8,9]. Since the indirect method converts X-ray photons into visible light photons and absorbs

them, the optical properties of the photon-charge conversion layer (called the active layer) are important. Inorganic materials mainly used in the active layer are expensive and difficult to form, thus research on X-ray detectors with organic materials whose optical properties are easy to change is in progress [10].

In this study, the active layer uses an organic semiconductor material that can be manufactured simply by solution processes, such as bar coating, spin coating, and inkjet printing. The organic layer is a bulk-heterojunction structure, in which a donor and an acceptor are mixed. Poly [[4,8-bis[5-(2-ethylhexyl)-2-thienyl]benzo[1,2-b:4,5-b'] dithiophene-2,6-diyl]-2,5-thiophenediyl[5,7-bis(2-ethylhexyl)-4,8-dioxo-4H,8H-benzo[1,2-c:4,5-c']dithiophene-1,3-diyl]] (PBDB-T), which has long chains and quinoids, has few charge traps and excellent carrier mobility [11,12], is used as a donor, while the commonly used (6,6)-phenyl C₇₁ butyric acid methyl ester (PC₇₁BM) is used as an acceptor, because it allows the formation of efficient bulk-heterojunctions to dissolve together with the donor polymer in common solvents [13]. However, the PC₇₁BM acceptor has weak absorbance and is a fullerene derivative having a bucky-ball structure, thus there is a problem with poor mechanical stability [14,15]. Therefore, the fullerene acceptor is unsuitable for application to flexible detectors, so the replacement by a non-fullerene acceptor (NFA) should be considered in a structurally stretched and unfolded network structure. Among several non-fullerene acceptors, 3,9-bis(2-methylene-(3-(1,1-dicyanomethylene)-indanone))-5,5,11,11-tetrakis(4-hexylphenyl)-dithieno[2,3-d:2',3'-d']-s-indaceno[1,2-b:5,6-b'] dithiophene (ITIC) was used. ITIC has a push-pull structure in terms of chemical structure, and exhibits excellent properties, as well as carrier transport and light absorption [16]. As can be seen from the energy band diagram in Figure 1, the difference between the lowest unoccupied molecular orbital (LUMO) and highest unoccupied molecular orbital (HOMO) of ITIC and PBDB-T is within 0.4 eV, which reduces the exciton separation energy loss generated in the active layer compared to PC₇₁BM, and could thereby improve the separated charge transferability [17]. The excitons generated from the donor by the visible photons were diffused and separated at the interface between the donor and the acceptor. After dissociation, electrons moved to the lithium fluoride/aluminum (LiF/Al) cathode and holes moved to the indium-tin-oxide (ITO) anode. To fabricate and evaluate a flexible organic radiation detector, the basic characteristics of glass, PEN, and CPI substrates were evaluated, the device was fabricated, and its performance was compared and evaluated through mechanical bending tests.

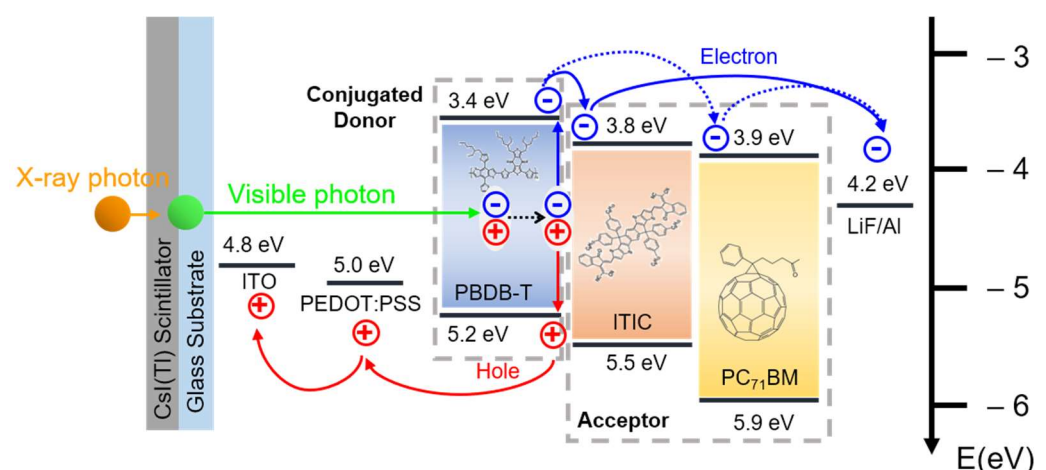


Figure 1. Energy band-diagram of the proposed organic X-ray detector with different acceptors as PC₇₁BM and ITIC.

2. Experiment Set-Up

Figure 2a,b shows the organic X-ray detector fabrication process flow and detector image on glass and CPI substrate. The substrates on which the 2 × 2 mm² active area was formed with a polyimide insulator on ITO patterned substrate was cleaned in an

ultrasonic cleaner. For the glass and PEN substrate, acetone, methanol, and IPA were used, while the CPI substrate used only IPA. After being cleaned, it was baked in a vacuum oven for 10 min. UV-ozone treatment was performed to hydrophilize the surface of the ITO patterned substrate. Poly(3,4-ethylenedioxythiophene): poly(styrenesulfonate) (PEDOT:PSS) with dimethylformamide (DMF) as the hole transport layer (HTL) was spin-coated onto the ITO patterned substrate under 3000 rpm spin-rate condition. The thickness of the HTL was about 30 nm. The active layer solution was prepared by mixing PBDB-T and PC₇₁BM (or ITIC) in a blend ratio of 1:1 using chlorobenzene solvent at a concentration of 20 mg/mL [18] and then spin-coated onto the HTL under 1100 rpm and 2500 rpm spin-rate conditions, respectively. The thickness of the PBDB-T:PC₇₁BM and PBDB-T:ITIC was about 100 nm [19,20]. After that, it was baked on the hot plate for 10 min. LiF/Al (0.5/120 nm in thickness) as the cathode was deposited using thermal evaporation under a pressure of 10^{-7} torr. Finally, soda-lime glass was used as a cover material, and it was fixed with a UV-hardened sealant to prevent moisture and oxygen in the air.

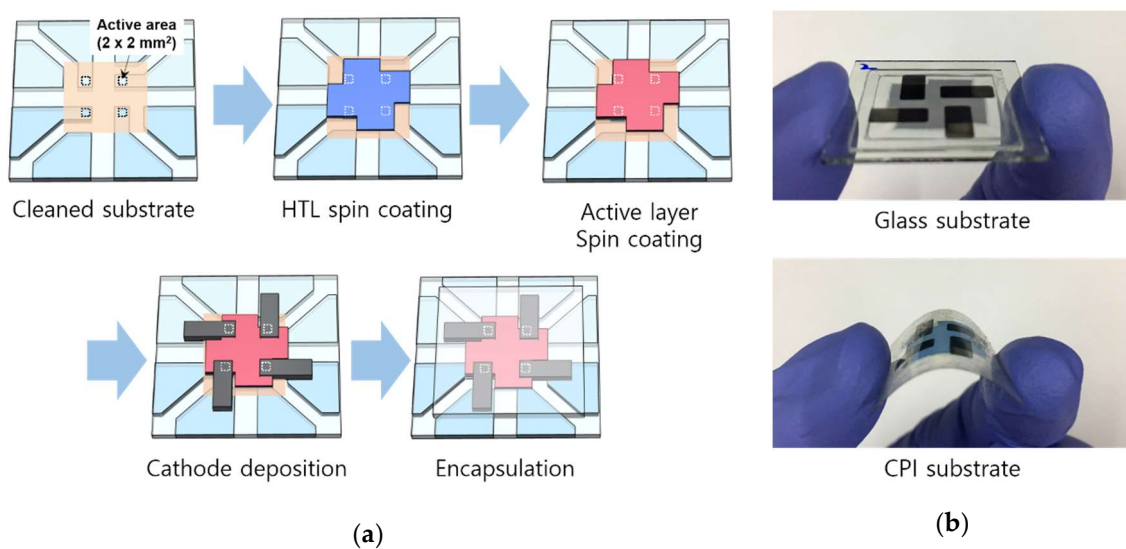


Figure 2. (a) Fabrication process of organic detector, and (b) images of fabricated detector on glass and CPI substrate.

Figure 3 shows the set-up for evaluating the flexible detector. After the bending test in a nitrogen atmosphere, soda-lime glass was attached to the detector for evaluation. A detector basically behaves similarly to a photodetector. Therefore, the evaluation method differs depending on the use or non-use of a scintillator that converts X-ray photons into visible-light photons. First, the scintillator-decoupled photodetector characteristics were evaluated using a solar simulator (San Ei Electronic, XES-40S2-CE). The detector was exposed to an AM 1.5 G filtered Xe lamp with 100 mW/cm^2 illumination conditions, to extract generated current density–applied voltage (J–V) curves by applying a bias of -1.0 to $+1.0$ V. The detector without scintillator parameters for evaluation, such as short circuit density (J_{SC}) and series resistance (R_S) were calculated from the J–V curve. Then, the X-ray detector property of coupling the CsI(Tl) scintillator composed of 0.5 mm of aluminum and 0.4 mm of CsI(Tl) (rigid type Hamamatsu J13113 or flexible type Hamamatsu J1477) was measured using an X-ray generator (AJ-2000H, AJEX) and a source meter (Keithley 2400). The device and the CsI(Tl) scintillator were coupled using a jig. The X-ray operation condition was fixed with a voltage of 80 kVp, current of 63 mAs, and irradiation time of 1.57 s. The X-ray generator anode material was tungsten and the total filtration was 2.8 mm thickness aluminum equivalent. The voltage of -0.6 V was applied to the detector anode (ITO) and cathode (LiF/Al) to collect the generated charges. The collected current density (CCD) was measured during the X-ray irradiation, while the dark current density (DCD) was measured without X-ray irradiation. The detection sensitivity, which is related to the

photon-to-charge conversion efficiency, is an important factor of the X-ray detector, and was calculated using the following equation:

$$\text{CCD } (\mu\text{A}/\text{cm}^2) = (\text{current during X-ray irradiation ON})/\text{Detection Area} \quad (1)$$

$$\text{DCD } (\mu\text{A}/\text{cm}^2) = (\text{current during X-ray irradiation OFF})/\text{Detection Area} \quad (2)$$

$$\text{Sensitivity } (\text{mA}/\text{Gy}\cdot\text{cm}^2) = (\text{CCD} - \text{DCD})/\text{Absorbed Dose} \quad (3)$$

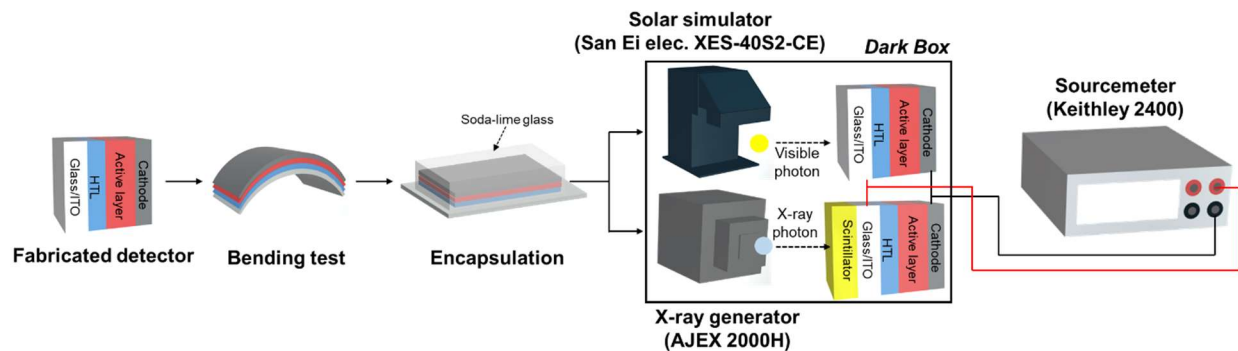


Figure 3. Experimental set-up of measuring the photodetector parameters of the scintillator decoupled detector, and the X-ray parameters of the scintillator coupled photodetector.

The mechanical flexibility and stability of the X-ray detector were measured using the bending machine. The degradation of detector performance was measured under different bending curvature (R) and bending cycle times. The bending curvature (R) was calculated according to Equation (4):

$$R \text{ (mm)} = (c^2 + 4h^2)/8h \quad (4)$$

where, c is the curved distance of the bended detector and h is the curved height.

3. Results and Discussion

3.1. Experiments for Substrates Comparison

The properties of rigid glass substrates and plastic substrates, such as PEN and CPI, were compared. Figure 4a,b shows the deformation curvature and sheet conductivity of the substrate according to temperature. The glass transition temperature (T_g) of the PEN substrate is about 160 °C, and when the heat of 150 °C is applied, the substrate begins to deform. Therefore, as the deformation curvature increases with increasing temperature, the sheet conductivity drops sharply. On the other hand, since the T_g of glass an CPI substrate is more than 300 °C, the temperature-dependent deformation curvature and deterioration of the surface conductivity properties are low. In general, since the firing temperature of the organic active layer is about 150 °C, it is important that the plastic substrate does not deform at a temperature below that. In addition, the transmittance of the substrate is also important for flexible detector applications. UV-Visible spectrophotometry (Optizen 2120UV) was used to show the transmittance according to the wavelength of each substrate, which is shown in Figure 4c. The transmittance of the CPI substrate in the visible light region is higher than that of the PEN substrate, and it is competitive, because it is similar to that of the glass substrate. According to the temperature-dependent deformation curvature, surface conductivity, and transmittance, if CPI substrate is used instead of a glass substrate, performance similar to that of a rigid organic material detector can be expected.

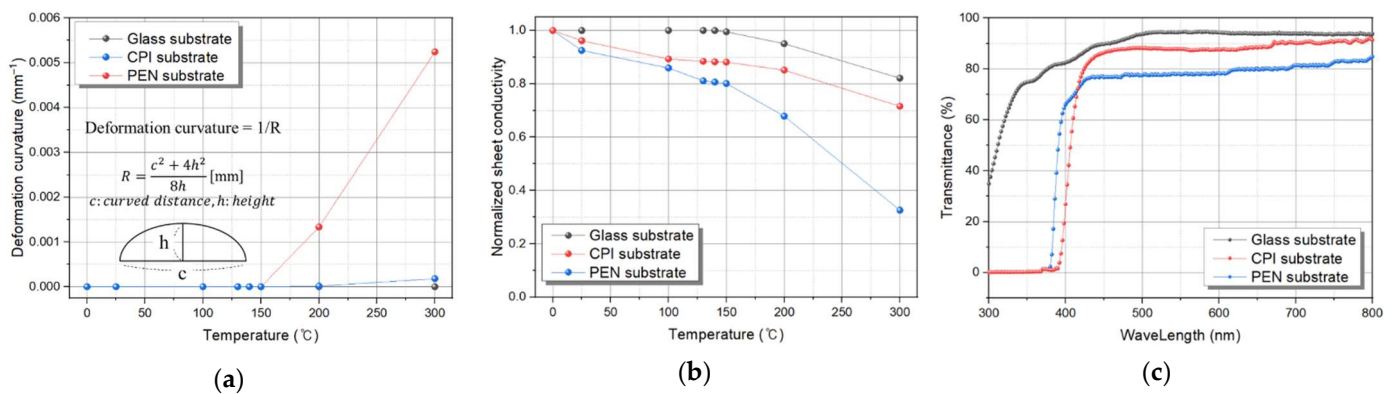


Figure 4. (a) Deformation curvature of glass, PEN, and CPI plastic substrate, (b) sheet conductivity of the substrates according to heat temperature, and (c) transmittance of substrates.

To evaluate the characteristics of each substrate, a device was manufactured using glass, PEN, and CPI, and the active layer was composed of PBDB-T as donor, and PC₇₁BM as acceptor. Figure 5a shows the J–V curve of the photodetector without the CsI(Tl) scintillator, and parameters, such as *J*_{SC} and *R*_s, were extracted from the detector J–V curve by J–V curve when an AM 1.5 G filtered Xe lamp with 100 mW/cm² illumination conditions and voltages from –1 to +1 V were biased. The electrical characteristic, *J*_{SC}, of the photodetector with PBDB-T:PC₇₁BM (glass, PEN, CPI), was 12.68, 12.23, and 11.09 mA/cm², respectively. Based on the glass substrate, the CPI substrate photodetector decreased by 3.55%, and the PEN substrate decreased by 12.54%. As an indicator of the uniformity of the active layer formation, *R*_s was 199.15, 204.20, and 322.17 Ω, respectively. The CPI was 2.54%, and PEN was increased by 61.77%, compared to the glass substrates. CCD, DCD, and sensitivity were measured by combining a rigid CsI(Tl) scintillator and a photodetector to which –0.6 V was biased under the X-ray operating conditions of 80 kVp tube voltage, 63 mAs tube current, and irradiation time of 1.57 s, as shown in Figure 5b. For the X-ray detector characteristics, the CCD of the CPI substrate decreased by 2.81%, and the sensitivity decreased by 4.07%, while the PEN substrate showed a decrease of 5.61% and 12.79%, respectively, based on the glass substrate. Compared to the glass and CPI substrates, the PEN substrates X-ray detector characteristics show relatively high degradation due to low *J*_{SC} and high *R*_s. Therefore, the application of CPI substrate is competitive in the flexible detector, because it shows similar characteristics to the glass substrate.

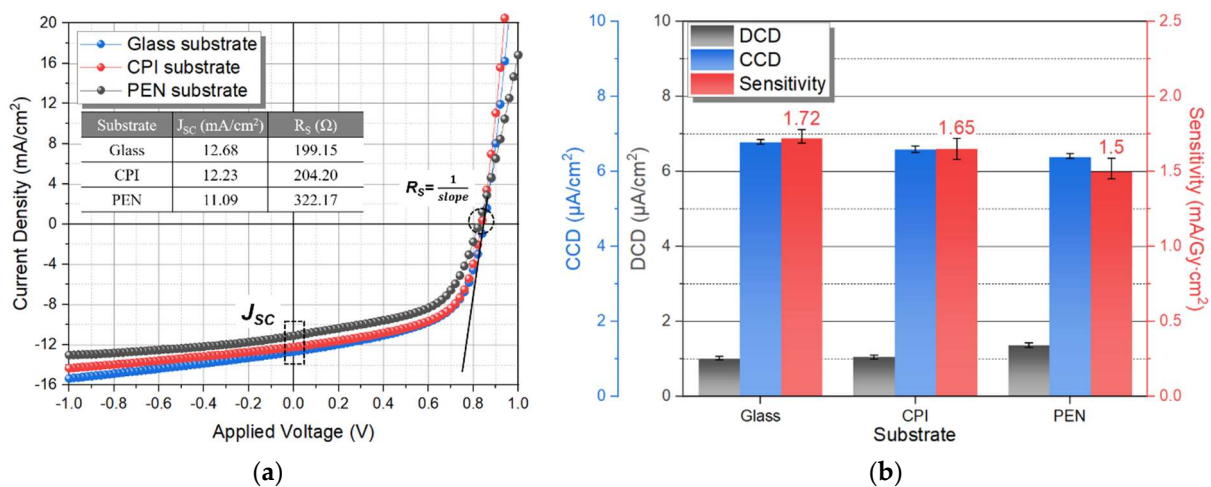


Figure 5. (a) J–V characteristics of photodetector with the PBDB-T:PC₇₁BM active layer, and (b) CCD, DCD, and sensitivity of the X-ray detector on glass, CPI, and PEN substrates.

3.2. Characteristics Experiment According to the Type of Acceptor Materials

According to the evaluation of devices manufactured using various substrates, the CPI substrate was fixed for flexible devices implementation, and experiments were conducted on different types of acceptors. The previously used PC₇₁BM is a three-dimensional structure of a buckyball with fullerene derivatives, which has the disadvantages of high synthesis cost, low extinction coefficient, and low mechanical stability [21]. On the other hand, ITIC as a two-dimensional non-fullerene network structure has the advantages of mechanical stability, high carrier transport, and light absorption characteristics. Therefore, the PC₇₁BM and ITIC acceptors were compared to find suitable materials for flexible detectors. The film condition was evaluated before application to the detector, and Figure 6a shows the AFM image. Through the AFM evaluation, the average surface roughness (R_q) was 1.14 nm and 2.59 nm, respectively, depending on the different acceptors (PC₇₁BM and ITIC), and Figure 6b shows other parameters, namely, R_s and J_{SC} . As the R_q increases, the surface area for absorption increases, but the R_s including the surface resistance tends to increase, which as a result increases the R_s of the detector with the PBDB-T:ITIC active layer. The R_s was 204.2 Ω and 567.7 Ω according to the different acceptors. However, the J_{SC} of the detector with PBDB-T:ITIC was 16.02 mA/cm², which shows a 31.10% improvement, compared to that of the detector with PBDB-T:PC₇₁BM of 12.22 mA/cm².

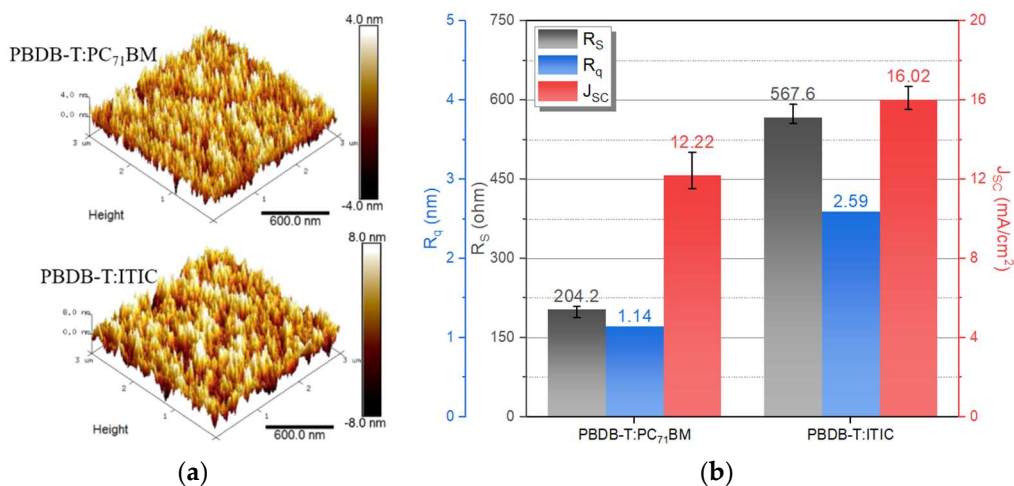


Figure 6. (a) AFM images of the organic active layer films, (b) average surface roughness (R_q), R_s , and J_{SC} with different acceptors (PC₇₁BM and ITIC).

To verify the reason for the increase in R_q and R_s while the electrical properties improved, the electron-transport properties of the detectors according to different receptors were characterized, and the J–V curve of the detector with a bias voltage of –3 to +3 V under dark condition was shown in Figure 7a. Using curve fitting of the logarithmic J–V curve, the electron mobility (μ) and defect density were calculated using the space charge limited current (SCLC) model [22–25], using the Mott–Gurney Equation (5), and following the defect density Equation (6):

$$\text{Carrier Mobility } (\mu) = (8/9) \times J \times (L^3 / (V_a^2 \cdot \epsilon_0 \cdot \epsilon_r)) \quad (5)$$

$$N_{\text{defect}} \text{ (Defect Density)} = (2 \cdot \epsilon_0 \cdot \epsilon_r \cdot V_{\text{FTL}}) / (q \cdot L^2) \quad (6)$$

where J is the current density and L is the thickness of the active layer (PBDB-T:PC₇₁BM and ITIC) measured using a surface profiler (KLA-Tencor Alpha-step AS-500). The V_a is the applied voltage in the SCLC region, ϵ_0 is the free-space permittivity constant of the vacuum (8.85×10^{-12} F/m), the relative permittivity (ϵ_r) of the PBDB-T:PC₇₁BM and PBDB-T:ITIC were 3.56 and 3.78, respectively [26]. The q is the elementary charge (1.602×10^{-19} C), and

V_{FTL} is defined as the trap-filled limit voltage, which is the voltage at the point where the trap-limited SCLC region and the trap-filled limit region overlap on the log scale J–V curve.

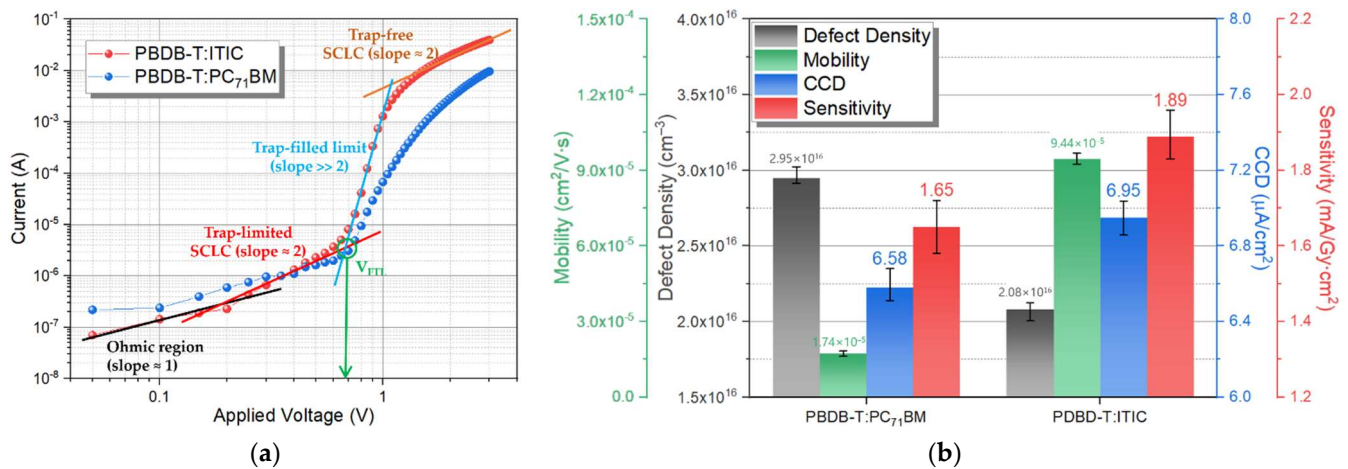


Figure 7. (a) Curve fitting of the logarithmic J–V characteristics, and (b) the mobilities, defect densities, CCD, and sensitivity of the as-prepared detector with the different acceptors under the dark condition.

The hysteresis according to the before and after X-ray irradiation of the fabricated detectors were measured, and it is shown in Figure S1. Figure 7b shows the mobility and defect density extracted from the Figure 7a graph measured in the dark condition to evaluate the charge-transfer characteristics of the fabricated detector. It also shows the CCD and sensitivity under X-ray irradiation condition, which is biased -0.6 V to the detector. The defect density is estimated to be 2.95 cm^{-3} and 2.08 cm^{-3} for the detector with PC_{71}BM and ITIC acceptors, respectively. In addition, the electron mobility extracted from the detector with different acceptors was improved by 442.53% from 1.74 to $9.44 \text{ cm}^2/\text{V}\cdot\text{s}$ for the PC_{71}BM to ITIC acceptor, respectively. This is because the network structured ITIC lowers the recombination of charges in the active layer, and improves the electron mobility, due to the higher carrier transfer characteristics, compared to PC_{71}BM . Therefore, when compared to the detector with PC_{71}BM and ITIC acceptors, the surface roughness and R_S were increased, but the electrical property of J_{SC} was improved. After coupling the rigid CsI(Tl) scintillator with the photodetector, the CCD and sensitivity were evaluated. CCD was extracted from the X-ray detector with PC_{71}BM and ITIC of $6.58 \text{ }\mu\text{A}/\text{cm}^2$ and $6.95 \text{ }\mu\text{A}/\text{cm}^2$ increase, respectively, due to the improvement of electrical properties, which is associated with the calculation of sensitivity, which showed a 14.55% increase from 1.65 to $1.89 \text{ mA}/\text{Gy}\cdot\text{cm}^2$, respectively. Therefore, the surface roughness of the PBDB-T:ITIC active layer was non-uniform and the resistance higher than that of the PCBM acceptor, but it was confirmed that the detector performance was improved due to the improvement of the electrical properties, and the flexibility test was then evaluated.

A flexible scintillator was used to implement the flexible X-ray detector, as shown in Figure S2. When the flexible scintillator was applied, the sensitivity was $1.95 \text{ mA}/\text{Gy}\cdot\text{cm}^2$. The sensitivity of the proposed flexible detector and several flexible detector studies were compared and shown in Table S1 in the supplementary file.

3.3. Bending Curvature and Bending Cycle Experiments for Flexibility Evaluation

After evaluating the photodetector and X-ray detector according to the different acceptors, the characteristics were evaluated, such as the bending curvature (R) and bending cycles. First, Figure 8a,b shows the J–V curve of the photodetector with the PBDB-T: PC_{71}BM and ITIC active layer according to the bending curvature test that was conducted. As the R increases, the characteristics of the device with PC_{71}BM acceptor deteriorates sharply at $R = 10$, while the device with the ITIC acceptor shows a relatively low decrease. Table 1

shows the detector without scintillator parameters extracted from Figure 8a,b of J_{SC} and R_S , respectively. J_{SC} values of the PCBM acceptor were 12.22 mA/cm², 11.72 mA/cm², 7.57 mA/cm², and 6.83 mA/cm² with degradation of up to 44.11% according to the bending curvature, while the R_S showed increase from 204.20 to 2604.55 Ω by 1175.49%. Meanwhile, the ITIC acceptor showed relatively low deterioration in J_{SC} by a decrease of 11.92% of $R = 2$, compared to the flat bending curvature, and an increase in R_S by 106.10%. As a result of the different acceptor characteristics, the 3D structure of PCBM has low stability of forming an active layer, which is brittle according to the physical bending, and the detector performance deteriorates rapidly, whereas ITIC has an unfolded structure, and is relatively more flexible than PC₇₁BM, thus ITIC is suitable for the flexible detector.

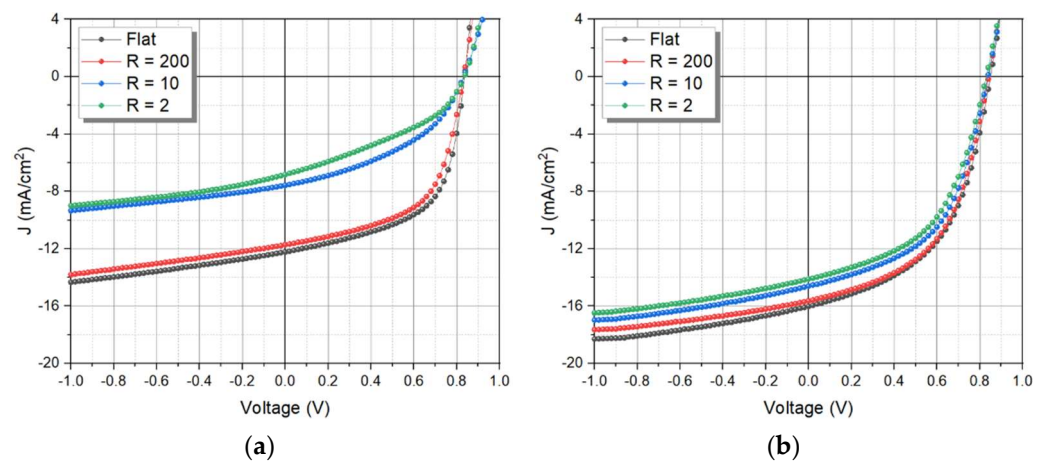


Figure 8. J–V characteristic of the detector according to bending curvature (a) with PBDB-T:PC₇₁BM, and (b) PBDB-T:ITIC, fixed at 50 times bending cycle.

Table 1. The parameters of detector without CsI(Tl) scintillator according to different acceptors (PC₇₁BM and ITIC).

Active Layer	Bending Curvature	J_{SC} (mA/cm ²)	R_S (ohm)
PBDB-T:PC ₇₁ BM	Flat	12.22	204.20
	R = 200	11.72	479.43
	R = 10	7.57	1925.18
	R = 2	6.83	2604.55
PBDB-T:ITIC	Flat	16.02	567.60
	R = 200	15.64	617.41
	R = 10	14.61	851.14
	R = 2	14.11	1169.84

The flexible X-ray detector was evaluated by combination with a flexible CsI(Tl) scintillator after the bending curvature experiment of the photodetector to measure the normalized sensitivity, as shown in Figure 9a. As the bending curvature decreased, the sensitivity of the ITIC detector decreased by 3.26%, 7.07%, and 6.52% from flat to $R = 200$, 10, and 2, respectively. On the other hand, the sensitivity of the PC₇₁BM detector is reduced by 5.46%, 18.18%, and 12.12%, which is much higher compared to the ITIC acceptor. Among them, normalized sensitivity showed a 46.82% difference in comparison with $R = 10$ according to the different acceptors, which showed a significant decrease in performance, and a 61.83% difference at $R = 2$. Next, a bending cycle experiment was performed by fixing the bending curvature of $R = 10$, the performance of which was significantly reduced, and Figure 9b shows the results. As the bending cycle increases, the performance deteriorates due to the continuous mechanical stress, and when increasing the bending cycle from 100 to 500 times, the normalized sensitivity of the X-ray detector with the PPBDB-T:PC₇₁BM active layer was 13.78% and the PBDB-T:ITIC active layer was 3.42%, showing relatively

low degradation characteristics. Under the condition of bending curvature of 10 mm^{-1} and bending cycle of 500 times, the X-ray detector with PBDB-T:ITIC shows 135.85% higher performance than the PBDB-T:PC₇₁BM active layer, thus a non-fullerene structured material, such as ITIC, is suitable as an acceptor for the flexible X-ray detector.

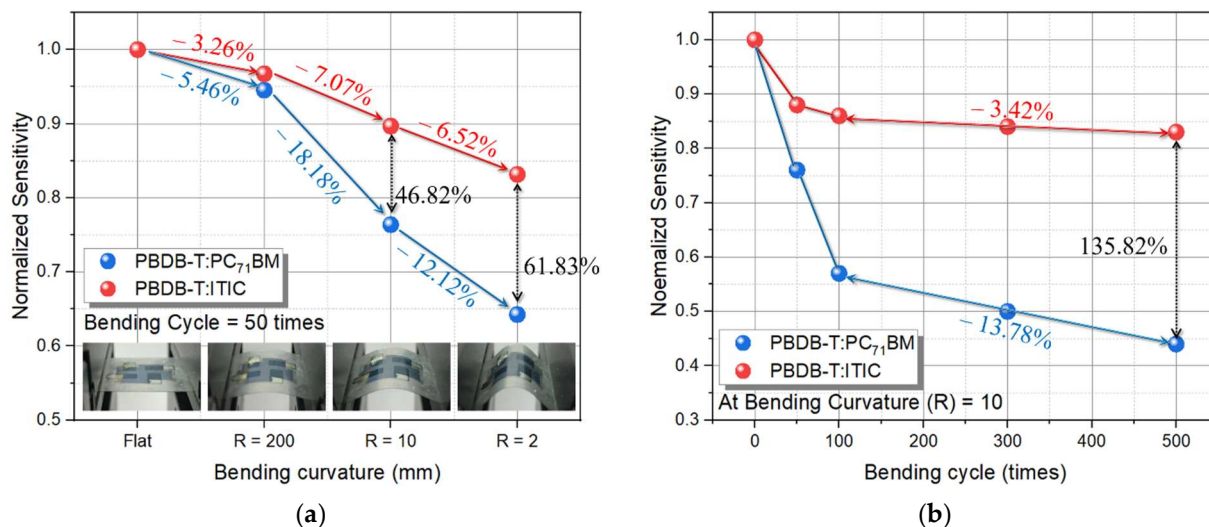


Figure 9. Normalized sensitivity degradation of the X-ray detectors as a function of (a) bending curvature, and (b) bending cycle times.

4. Conclusions

In this study, we investigated the characteristics of the colorless polyimide (CPI) film-based flexible X-ray detector. Plastic substrates, such as polyethylene terephthalate (PET), polyethylene naphthalate (PEN), and polyimide (PI), were mainly used for the flexible devices. The CPI film has an advantage in sensor applications, because it shows excellent transmittance by removing the yellow color from PI, which has physical and chemical stability. In addition, compared with the PEN substrate with high thermal stability, the deformation curvature according to the temperature showed similar characteristics to that of the glass substrate. Therefore, CPI was applied to the proposed flexible X-ray detector, due to having flexibility and similar characteristics to the glass substrate. The active layer of the detector was composed of an organic donor, such as poly[(2,6-(4,8-bis(5-(2-ethylhexyl)thiophen-2-yl)-benzo[1,2-b:4,5-b']dithiophene))-alt-(5,5-(1',3'-di-2-thienyl-5',7'-bis(2-ethylhexyl)benzo[1',2'-c:4',5'-c']dithiophene-4,8-dione)] (PBDB-T), and an acceptor, such as (6,6)-phenyl C₇₁ butyric acid methyl ester (PC₇₁BM), as a bulk-heterojunction (BHJ). However, PC₇₁BM is a three-dimensionally (3D) bucky-ball structure that is easily broken by physical bending, so that is not suitable for flexible devices and has the disadvantage of low morphological stability in mixed organic materials. Therefore, the PC₇₁BM acceptor was replaced with a non-fullerene acceptor, such as ITIC, with a two-dimensionally unfolded structure, and has high carrier transport and light absorption characteristics. The detection sensitivity of the detector with PBDB-T:ITIC was higher than that of PBDB-T:PC₇₁BM by 11.18%. The mechanical stability evaluation of the flexible detector measured the decrease in detection sensitivity through the bending curvature (R) and the bending cycle. First, the normalized sensitivity of the detector using the PBDB-T:ITIC active layer was 46.82% better than that using the PBDB-T:PC₇₁BM active layer at the bending curvature of 10 mm^{-1} , by fixing the 50 times bending cycle. Second, the normalized sensitivity change was measured according to the bending cycle 500 times with the bending curvature fixed at $R = 10$, where the detector using the PBDB-T:ITIC active layer decreased by 3.42%, and that using the PBDB-T:PC₇₁BM active layer decreased by 13.78%; and the normalization sensitivity of the PBDB-T:ITIC active layer gives better

results by 135.85%. Therefore, the non-fullerene acceptor ITIC is more suitable for a flexible device, because it has better mechanical flexibility than PC₇₁BM.

Supplementary Materials: The following supporting information can be downloaded at: <https://www.mdpi.com/article/10.3390/nano12060918/s1>, Figure S1: J-V characteristic hysteresis measured at dark conditions, before and after X-ray irradiation to the detector using (a) PBDB-T:PC₇₁BM and (b) PBDB-T:ITIC active layer.; Figure S2: (a) Emission spectrum of the rigid and flexible CsI (TI) scintillator under the same X-ray condition, and (b) the CCD and sensitivity of the X-ray detector with different scintillators.; Table S1: The performance comparison of flexible X-ray detectors [27–31].

Author Contributions: Conceptualization, J.K.; formal analysis, J.L., D.L. and J.K.; investigation, J.L., J.W. and J.K.; data curation, J.L., D.L. and J.K.; writing—original draft preparation, J.L., J.W. and H.L.; writing—review and editing, J.L., J.W., H.L. and J.K.; visualization, J.L., J.W. and H.L.; supervision, J.K.; project administration, J.K.; funding acquisition, J.K. All authors have read and agreed to the published version of the manuscript.

Funding: This work was supported by a Korea Institute for Advancement of Technology (KIAT) grant funded by the Korea Government (MOTIE) (P0017011, HRD Program for Industrial Innovation).

Institutional Review Board Statement: Not applicable.

Informed Consent Statement: Not applicable.

Data Availability Statement: The data is included in the main text and the supplementary materials.

Conflicts of Interest: The authors declare no conflict of interest.

References

1. Sun, Y.; Chang, M.; Meng, L.; Wan, X.; Gao, H.; Zhang, Y.; Zhao, K.; Sun, Z.; Li, C.; Liu, S.; et al. Flexible organic photovoltaics based on water-processed silver nanowire electrodes. *Nat. Electron.* **2019**, *2*, 513–520. [[CrossRef](#)]
2. Jeon, Y.; Choi, H.R.; Lim, M.; Choi, S.; Kim, H.; Kwon, J.H.; Park, K.C.; Choi, K.C. A Wearable Photobiomodulation Patch Using a Flexible Red-Wavelength OLED and Its In Vitro Differential Cell Proliferation Effects. *Adv. Mater. Technol.* **2018**, *3*, 1700391. [[CrossRef](#)]
3. Pak, K.; Choi, J.; Lee, C.; Im, S.G. Low-Power, Flexible Nonvolatile Organic Transistor Memory Based on an Ultrathin Bilayer Dielectric Stack. *Adv. Electron. Mater.* **2019**, *5*, 1800799. [[CrossRef](#)]
4. Liang, H.; Cui, S.; Su, R.; Guan, P.; He, Y.; Yang, L.; Chen, L.; Zhang, Y.; Mei, Z.; Du, X. Flexible X-ray Detectors Based on Amorphous Ga₂O₃ Thin Films. *ACS Photon.* **2019**, *6*, 351–359. [[CrossRef](#)]
5. Yin, Z.; Sun, S.; Salim, T.; Huang, X.; He, Q.; Lam, Y.M.; Zhang, H. Organic Photovoltaic Devices Using Highly Flexible Reduced Graphene Oxide Films as Transparent Electrodes. *ACS Nano* **2010**, *4*, 5263–5268. [[CrossRef](#)] [[PubMed](#)]
6. Lee, J.; Kang, J. Characteristics of a Flexible Radiation Detector Fabricated with Non-Fullerene Acceptor for an Indirect-type X-ray Imaging. *J. Instrum.* **2019**, *14*, C03008. [[CrossRef](#)]
7. Lee, D.H.; Yun, H.; Jung, E.D.; Chu, J.H.; Nam, Y.S.; Song, S.; Seok, S.H.; Song, M.H.; Kwon, S.Y. Ultrathin Graphene Intercalation in PEDOT:PSS/Colorless Polyimide-Based Transparent Electrodes for Enhancement of Optoelectronic Performance and Operational Stability of Organic Devices. *ACS Appl. Mater. Interfaces* **2019**, *11*, 21069–21077. [[CrossRef](#)]
8. Kim, B.; Lee, J.; Kang, J. Improving the sensitivity of indirect-type organic X-ray detector by blending with CdSe quantum dots. *J. Instrum.* **2017**, *12*, C01009. [[CrossRef](#)]
9. Liu, H.; Lee, J.; Kang, J. Characteristics of A Hybrid Detector Combined with A Perovskite Active Layer for Indirect X-ray Detection. *Sensors* **2020**, *20*, 6872. [[CrossRef](#)]
10. Elandaloussi, E.H.; Frère, P.; Richomme, P.; Orduna, J.; Garin, J.; Roncali, J. Effect of Chain Extension on the Electrochemical and Electronic Properties of π -Conjugated Soluble Thienylenevinylene Oligomers. *J. Am. Chem. Soc.* **1997**, *119*, 10774–10784. [[CrossRef](#)]
11. Ma, Z.; Geng, H.; Wang, D.; Shuai, Z. Influence of alkyl side-chain length on the carrier mobility in organic semiconductors: Herringbone vs. π - π stacking. *J. Mater. Chem. C* **2016**, *4*, 4546–4555. [[CrossRef](#)]
12. Kleinhenz, N.; Yang, L.; Zhou, H.; Price, S.C.; You, W. Low-Band-Gap Polymers That Utilize Quinoid Resonance Structure Stabilization by Thienothiophene: Fine-Tuning of HOMO Level. *Macromol.* **2011**, *44*, 872–877. [[CrossRef](#)]
13. Kadem, B.; Al-Hashimi, M.K.; Hassan, A. The Effect of Solution Processing on the Power Conversion Efficiency of P3HT-based Organic Solar Cells. *Energy Procedia* **2014**, *50*, 237–245. [[CrossRef](#)]
14. Kim, T.; Kim, J.-H.; Kang, T.E.; Lee, C.; Kang, H.; Shin, M.; Wang, C.; Ma, B.; Jeong, U.; Kim, T.-S.; et al. Flexible, highly efficient all-polymer solar cells. *Nat. Commun.* **2015**, *6*, 8547. [[CrossRef](#)]

15. Holliday, S.; Ashraf, R.S.; Wadsworth, A.; Baran, D.; Yousaf, S.A.; Nielsen, C.B.; Tan, C.-H.; Dimitrov, S.D.; Shang, Z.; Gasparini, N.; et al. High-efficiency and air-stable P3HT-based polymer solar cells with a new non-fullerene acceptor. *Nat. Commun.* **2016**, *7*, 11585. [[CrossRef](#)]
16. Lin, Y.; Wang, J.; Zhang, Z.-G.; Bai, H.; Li, Y.; Zhu, D.; Zhan, X. An Electron Acceptor Challenging Fullerenes for Efficient Polymer Solar Cells. *Adv. Mater.* **2015**, *27*, 1170–1174. [[CrossRef](#)]
17. Bai, Y.; Yang, B.; Chen, X.; Wang, F.; Hayat, T.; Alsaedi, A.; Tan, Z. Constructing Desired Vertical Component Distribution Within a PBDB-T:ITIC-M Photoactive Layer via Fine-Tuning the Surface Free Energy of a Titanium Chelate Cathode Buffer Layer. *Front. Chem.* **2018**, *6*, 292. [[CrossRef](#)]
18. Xu, Y.; Yuan, J.; Zhou, S.; Seifrid, M.; Ying, L.; Li, B.; Huang, F.; Bazan, G.C.; Ma, W. Ambient Processable and Stable All-Polymer Organic Solar Cells. *Adv. Funct. Mater.* **2019**, *29*, 1806747. [[CrossRef](#)]
19. Won, J.; Liu, H.; Kang, J. Improvement of Indirect X-ray Detector Performance by Applying Additive Solvent to the Organic Active-Layer. *J. Nanosci. Nanotech.* **2021**, *21*, 2998–3003. [[CrossRef](#)]
20. Ban, D.; Yoo, K.; Kang, J. Characteristics of an organic photodetector with a conjugated donor and non-fullerene acceptor for indirect X-ray detection. *J. Instrum.* **2019**, *14*, P12012. [[CrossRef](#)]
21. Wei, J.; Tu, Q.; Zheng, Q. Heteroheptacene-cored semiconducting molecules for non-fullerene organic solar cells. *Dye. Pigment.* **2017**, *144*, 133–141. [[CrossRef](#)]
22. Kwan, C.-P.; Street, M.; Mahmood, A.; Echtenkamp, W.; Randle, M.; He, K.; Nathawat, J.; Arabchigavkani, N.; Barut, B.; Yin, S.; et al. Space-charge limited conduction in epitaxial chromia films grown on elemental and oxide-based metallic substrates. *AIP Adv.* **2019**, *9*, 055018. [[CrossRef](#)]
23. Jhamba, L.; Wamwangi, D.; Chiguvare, Z. Dependence of mobility and charge injection on active layer thickness of bulk heterojunction organic solar cells: PCBM:P3HT. *Opt. Quantum Electron.* **2020**, *52*, 245. [[CrossRef](#)]
24. Haneef, H.F.; Zeidell, A.M.; Jurchescu, O.D. Charge carrier traps in organic semiconductors: A review on the underlying physics and impact on electronic devices. *J. Mater. Chem. C* **2020**, *8*, 759–787. [[CrossRef](#)]
25. Jahandar, M.; Khan, N.; Lee, H.K.; Lee, S.K.; Shin, W.S.; Lee, J.-C.; Song, C.E.; Moon, S.-J. High-Performance CH₃NH₃PbI₃-Inverted Planar Perovskite Solar Cells with Fill Factor Over 83% via Excess Organic/Inorganic Halide. *ACS Appl. Mater. Interfaces* **2017**, *9*, 35871–35879. [[CrossRef](#)]
26. Sareni, B.; Krähenbühl, L.; Brosseau, C.; Beroual, A. Effective dielectric constant of random composite materials. *J. Appl. Phys.* **1997**, *81*, 2375–2383. [[CrossRef](#)]
27. Heo, J.H.; Park, J.K.; Yang, Y.; Lee, D.S.; Im, S.H. Self-powered flexible all-perovskite X-ray detectors with high sensitivity and fast response. *iSci.* **2021**, *24*, 102927.
28. Li, Z.; Chang, S.; Hu, Y.; Huang, Y.; Au, L.; Ren, S. Flexible Lead-Free X-ray Detector from Metal-Organic Frameworks. *Nano Lett.* **2021**, *21*, 6983–6989.
29. Guo, J.; Xu, Y.; Yang, W.; Xiao, B.; Sun, Q.; Zhang, X.; Zhang, B.; Zhu, M.; Jie, W. High-Stability Flexible X-ray Detectors Based on Lead-Free Halide Perovskite Cs₂TeI₆ Films. *ACS Appl. Mater. Interfaces* **2021**, *13*, 23928–23935.
30. Mao, L.; Li, Y.; Chen, H.; Yu, L.; Zhang, J. A high-sensitivity flexible direct x-ray detector based on bi₂o₃/pdms nanocomposite thin film. *Nanomaterials* **2021**, *11*, 1832.
31. Shrestha, S.; Fischer, R.; Matt, G.J.; Feldner, P.; Michel, T.; Osvet, A.; Levchuk, I.; Merle, B.; Chen, H.; Tedde, S.F.; et al. High-performance direct conversion X-ray detectors based on sintered hybrid lead triiodide perovskite wafers. *Nat. Photonics.* **2017**, *11*, 436–440.